Proceedings of IPACK'01
The Pacific Rim/International Electronic Packaging
Technical Conference and Exhibition
July 8-13, 2001, Kauai, Hawaii, USA

IPACK2001-15620

RAPID SCALE-UP DESIGN OF A FORCED CONVECTION, RADIO FREQUENCY ABSORPTION LOAD USING FLOW NETWORK MODELING AND COMPUTATIONAL FLUID DYNAMICS

Joel D. Meltzer, Bird Electronic Corporation
Solon, OH, USA

Amir Radmehr, Ph.D., Innovative Research, Inc.
Plymouth, MN, USA

ABSTRACT

This study was performed to evaluate the scalability of an existing air-cooled, radio frequency (RF) absorption load design using system-level investigations with Flow Network Modeling (FNM) and detailed results from Computational Fluid Dynamics (CFD). The novelty of this study lies in the coupled application of FNM and CFD techniques to a high-power, digital broadcast load consisting of a validated RF absorption structure, existing air moving devices, and a tested system design which were scaled to develop a cooling chassis capable of increased RF power levels. Since design targets were well defined for the existing system, it was possible to use the FNM technique for rapid progression to the new, higher power design in the conceptual stage by evaluating sensitivities to cross-sectional area, free area ratio, air moving devices, and power levels. The FNM results were then used as a firm baseline for detailed CFD analysis, substantially reducing the number of time-consuming CFD iterations. This greatly shortened the design cycle and resulted in unprecedented time to market. In this paper, design considerations of air-cooled loads and the application of the FNM technique to their cooling design are discussed. FNM and CFD estimates of volumetric flow rates, average velocities, component pressure drops and global temperatures of the absorbing media are presented and compared with experimental data.

NOMENCLATURE

Zo: impedance (ohms)	f: frequency (Hz)
ε: permitvity (farad/m)	Re: Reynolds number
D, d: coaxial diameters (m)	Pr: Prandtl number
A: flow area (m^2)	a, m, n: empirical constants
RL: return loss (dB)	k: loss coefficient
α: attenuation (dB/m)	ρ : fluid density (kg/m^3)
Q: volumetric flow rate (CFM)	$VSWR$: voltage standing wave ratio

INTRODUCTION

Design engineers in the digital broadcast system market, as with the entire electronics industry, are finding that rapid time to market is an essential product specification. Producers of such equipment often must modify products rapidly to meet individual customer needs and adapt to changing specifications and standards. The so-called digital revolution in broadcasting has also added new design challenges for system design and packaging. This paper presents a design methodology that enabled rapid modification of a developed product to meet an immediate market need by Flow Network Modeling (FNM) and Computational Fluid Dynamics (CFD) techniques and physical validation in an extremely efficient and cost effective manner. This methodology will be illustrated by discussing a high-power, digital, air-cooled load designed to operate in the VHF frequency spectrum.

A load is defined as an impedance-matched device that absorbs propagating guided Electro-Magnetic (EM) energy and converts it to heat. Broadcast loads are typically used in four main applications: antenna simulation, standby power rejection, hybrid power combiners or dividers, and impedance isolators. The reader is referred to the substantial literature available discussing these applications [1]. Loads cooled entirely by forced air have the advantage of being able to run stand-alone without external cooling circuits and have a much longer maintenance cycle than other technologies. In addition, extremely high-absorbed peak powers are attainable due to large surface areas and they do not require cooling fluids or associated plumbing. They can also achieve a good frequency response, as air is the main dielectric. However, loads cooled entirely by forced convection have an inherent limit on maximum average absorbed power and have the lowest power density (watts absorbed per total package volume.)

In broadcast applications, the absorbed EM energy is most commonly converted into heat through a resistive structure, which are found in three types: bulk ceramic, thick film paste, and thin film pyrolitic. Bulk ceramic media consist of a sintered suspension containing resistive material and a ceramic binder, thick film pastes contain resistive materials and a binder mixture that is brushed or sprayed on a substrate, typically BeO or Al_2O_3 and thin film media use a ceramic substrate with a thin film of carbon applied by vacuum deposition. Detailed discussions of the limitations and manufacture of resistive structures can be found in the literature [2-4]. The choice of absorptive structure depends on several design criteria including peak power demands, operating temperature, fabrication costs, and frequency response.

DESIGN CONSIDERATIONS

Designing a load for digital broadcast presents unique challenges from both thermal and electrical design standpoints. Communication systems of all types are undergoing a transformation. The requirement for greater spectrum efficiency along with the need for more information transfer within a given bandwidth, has given rise to complex modulation schemes that are very different from traditional amplitude, frequency or phase related types. These new digital modulation systems give rise to waveforms that are fundamentally very different from waveforms resulting from older modulation methods. In the context of transmission component design, and specifically the design of loads, the most important parameter that has changed is the peak to average power ratio of the signal. In televisions systems, the current NTSC modulation scheme used primarily in the US as well as the PAL systems used in Europe have peak to average power ratios that do not exceed 2.2 dB. In new schemes such as 8-VSB (eight-level vestigial sideband) system used for HDTV in the US, or the COFDM (coded-orthogonal frequency division multiplex) system used for DTV in Europe (also for DAB in the US), typical peak to average power ratios exceed 8 dB. To further complicate matters, new systems often incorporate multiple transmitters feeding a single antenna. Peak to average ratios are higher still in these systems, where the peak to average power ratio will increase by 3dB each time the number of carriers is doubled.

When high peak-power signals are present upon a resistive structure, high thermal conductivity from the substrate alone is not as helpful since each instance of peak power from a digital signal results in localized heating and therefore high localized shear stresses which can result in de-lamination of the resistive film. Rather, a high thermal diffusivity is desirable to conduct the heat away as quickly as possible. Additional factors must also be considered to avoid peak-power breakdown including total area, length, and thickness of the resistive material. The peak power demands arising from digital modulation schemes also present concerns arising from increased voltage gradients. In general, increased distances between inner and outer conductor should be chosen where possible, and dielectrics with higher voltage breakdown including coolant fluids that may be present in the RF field should be employed. Larger surface areas of the resistive array are also desired in order to ensure lower energy density as well as a larger convective cooling area. Simply increasing the size and surface area of a high-power RF structure to accommodate digital modulation can, however, cause undesirable effects in the electrical design as the RF response of a structure is heavily dependent on its geometry and size. A fundamental constraint on the load geometry is the impedance of the load. Consider a simple coaxial transmission line of outer and inner conductor radius D and d. The characteristic impedance is given by:

$$Z_0 = \left(\frac{60}{\sqrt{\varepsilon}}\right) ln\left(\frac{D}{d}\right) \tag{1}$$

with Z_o typically 50, or 75 ohms for broadcast systems. The return loss, in dB, can be derived:

$$RL = -20\, log_{10}\left[\frac{(VSWR-1)}{(VSWR+1)}\right] \tag{2}$$

where the value of VSWR or voltage standing wave ratio is greater than 1.0 and a measure of the mismatch between the line and load, with a value of 1.0 representing a perfectly matched load. This gives rise to the well known result that the load impedance must be as closely matched as possible to the line impedance to minimize reflection. It follows that if a resistive structure forming one of the conductors is increased to meet aforementioned criterion for peak power, the corresponding dimensions in Equation 1 must be adjusted to maintain the match and broadband response of the load.

Avoiding the generation of the fundamental transverse electric mode (TE_{11}) is another design constraint with coaxial transmission lines and RF broadcast loads, thus the size of the transmission line or absorption structure must be chosen carefully. For a coaxial transmission line, the frequency at which the TE_{11} mode propagates is given by [5]:

$$f = \frac{300}{\pi\sqrt{\varepsilon}(D+d)} \tag{3}$$

however, the useful frequency range is typically 200-300 MHz less than the cut-off due to VSWR restrictions. While increasing the area would lower the power density and allow lower back-pressure due to increased cross-sectional area, the useful frequency range can be compromised.

Another design consideration is the non-uniform power distribution on the resistive structures found in attenuator designs. The attenuation of energy down the length of the transmission line is well known [6] and is expressed in dB/unit length:

$$\alpha = \left(\frac{\rho}{Z_0}\right)\left(\frac{1}{D}+\frac{1}{d}\right)\sqrt{f} \qquad (4)$$

The constant, ρ, is derived form the material properties of the transmission line and the dielectric between the conductors. For a copper line, α can range from 1x10E-5 dB/m to .03 dB/m. Clearly, the load needs to attenuate the power in as short a length as possible, on the order of 30-40 dB/m. Typically, one of the diameters or the impedance is varied along the length of the load, providing a decreasing attenuation relation with respect to distance. This results in both higher heating and higher voltage gradients of the RF absorption media at the input of the load as it has the highest power density (W/m^2).

Often loads must operate at high altitudes dictated by antenna and base-station placement. Altitudes of 10,000 ft or greater are not uncommon. Also extreme ambient conditions may occur at sites that are very remote or may not have adequate climate control. These environmental specifications are critical for air loads since the thermodynamic properties of air are affected. The load must be investigated in these extremes to ensure the temperature limits of the resistive media are not compromised and adequate flow rate is available.

ANALYSIS METHODOLOGY

A main goal of three-dimensional thermal and fluid simulations is to visualize, validate and optimize a design concept before physical prototypes are built and tested. Ideally, if correlations are good, one prototype may be all that is needed to validate engineering specifications. Constructing and analyzing these complex models using CFD, however, can be as time-consuming as physical prototyping and requires highly skilled personnel for effective use. Major changes to a design often require partial if not complete rebuilding of the element mesh and boundary conditions which can consume a large percentage of the total simulation time. Predicting what changes need to be investigated can reduce the re-meshing time if the simulation model is built with anticipation of these design changes. Rarely is this achievable unless the design changes are small. FNM takes this development cycle one step further by allowing the design engineer the ability to evaluate many design iterations quickly before a single CFD model is built, ultimately reducing the modeling cycles required with CFD. FNM differs from CFD in complexity, ease of use and level of detail produced. Several good references exist discussing the individual application of FNM as a robust design tool [7-9]. While the CFD technique along with thermal analysis with finite difference or finite element methods give an accurate picture of the temperature and flow characteristics, FNM allows rapid, first-order analysis of various design options and provides many answers to what-if scenarios in a rapid and inexpensive way.

A qualitative comparison of different design approaches is shown in Figure 1. The first method is a test-based process using hand-calculations (HC) to arrive at baseline values for cross-sectional area, AMDs, free-area ratios, etc and then proceeding to physical prototype testing. Clearly this is a very costly and time-consuming method often prohibiting new and creative iterations as the time and cost constraints more often drive the investigation. The second method utilizes a CFD-based analysis. Hand calculations still serve as the basis for the CFD model, however, the majority of iterations are performed on the CFD model, thereby reducing the number of physical prototypes and the time for final design. The third method shows an FNM-CFD based approach. Using this methodology, the FNM serves as a prerequisite to the CFD model. The majority of the design iterations are now performed with FNM, which not only reduces the number of CFD and physical prototype iterations but also the overall development time.

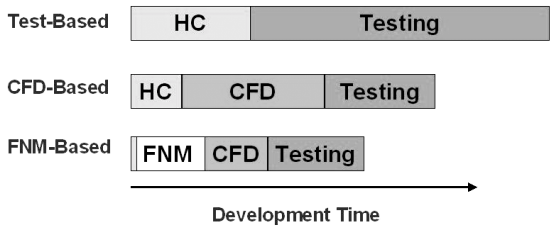

Figure 1: Qualitative Comparison of Development Methodologies

Driving the need for an efficient thermal design methodology was a short market opportunity, prompting the development of a new, digital-ready, VHF air-cooled load having the same electrical specifications as a 10kW baseline unit but with larger power handling capability. This baseline unit had previously been developed, prototyped, tuned and validated using a similar design methodology to design the RF sub-assembly. An electrical network model (ENM) was used to provide baseline values for modeling with a 3D, finite-element electro-magnetic solver which provided accurate predictions of return loss, and voltage gradients to verify peak-power margin. The RF subassembly was then built, tested and refined until specifications were met. Even with this design method realizing a significant time savings, a substantial portion of development time had been invested in the design of the RF section of the load and it was desired to leverage this as it could meet all of the electrical specifications for the scaled-up load. The scale-up of the 10kW unit to a 25kW unit would of course involve increasing the CFM through the system. During the thermal design portion of this product, the FNM-CFD-test methodology was used to reduce the thermal design effort and shorten time to market.

THE PHYSICAL SYSTEM

The overall design concept of the system under consideration is to direct the RF energy into an absorption structure suspended in a path of high-CFM airflow, which is exhausted to the exterior of the unit. Figure 2 shows an outline of the physical system under study. The RF absorption section consists of a series of optimized steps that transfer the RF energy from a standard coaxial transmission line to an array of energy absorbing resistors, configured to provide a return loss of 25-35 dB. The four identical outer air guides (OAG) provide separate pressure chambers that house the air moving devices (AMD), one for each chamber, which are feed by nozzle-shaped inlet rings (AIR_INLET). The air from the four AMDs enters the top of the RF inner housing through divided perforations (RF_INLET_SCREEN), combines, and passes over the resistor support structure (RESISTOR_LAUNCH), then the absorbing resistors, contained in the RF inner housing (RF_INNER_HOUSING) thus providing forced convection cooling. The inner housing has a three-fold purpose: first as an inner guide for the cooling air, second as the outer conductor ground path for the RF circuit, and third as a secondary RF shield in addition to the outer case preventing EM radiation leakage. The air heated by the resistor array enters the duct/diffuser (DUCT01 & DUCT02) and exits through a mesh screen (EXHAUST). This exit screen also serves to contain RF leakage.

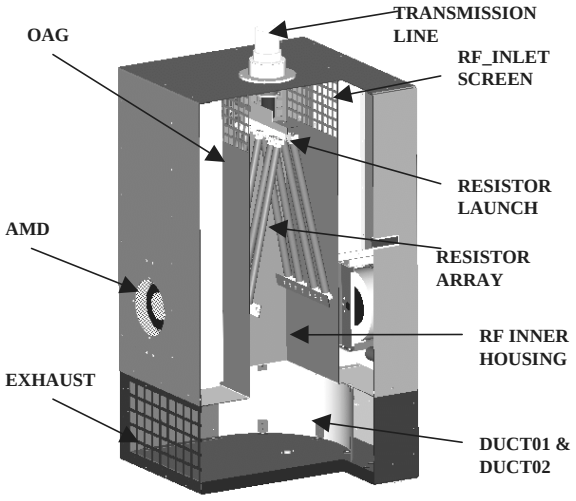

Figure 2. The Physical System

DESIGN GOALS

In addition to standard design features such as low cost, high reliability, etc., a well-designed digital broadcast air load will have the following characteristics:

- High return loss (power absorption) - stable over temperature
- Cool exterior temperatures
- Small size
- No radiation leakage
- Peak power capacity arising from digital modulation (10 dB)
- Broadband frequency response i.e. 50 + j0 ohms.
- Mountable in any position
- Capable of interfacing to standard transmission lines
- Margin for increased ambient temperature, altitude, and back-pressure due to external ducting

One of the critical design goals was to preserve the electrical characteristics, of the scaled-up load without investing in re-development of the RF section. Clearly the re-use of the prior RF design would be a key factor to meet the time to market window. It was desired to provide all the key features of the baseline, 10kw unit with the increased power demands. In addition to the desired features discussed in above, the following specifications would need to be realized to meet customer specifications, time to market and cost of goods targets:

- 25 kW average, 10 dB peak RF power capability
- Preserve VSWR and frequency of operation from baseline
- 1500 total CFM at 60 Hz. line frequency
- Use AMD sub-assemblies from similar product families
- Average velocity greater than 10 m/sec at the start of the absorption array
- Average resistor temperatures less than 500 degrees C
- Margin for ambient of +45 degree C and 50 Hz line frequency
- Have overall package size smaller than 30L” x 30W” x 60H”

Through 3D EM simulations and legacy data from similar RF structures, it was determined that the current RF section would be capable of handling the increased power levels, contingent on proper cooling design. This would be a pivotal time saving as it would allow the 10kW RF design to be reused with the main requirement of increasing the CFM through the system. The requirement for increased volumetric airflow would normally dictate increasing the area of the RF chamber. But, as outlined above, this would certainly cause the scaled-up unit to fail its’ electrical specifications, and require costly re-development. Therefore, validating the achievable CFM through the existing RF subassembly was an immediate goal. It was also desired to obtain this increased CFM by using existing AMDs and packaging, thus saving on prototype fabrication. The velocity specification at the start of the absorption array is dictated by the non-uniform heating on the resistor array

discussed previously. It was calculated that this average velocity would provide the necessary convection coefficient to adequately cool the top portion of the resistive array. Resistor temperature limits are determined by the material choices used in the unit. Exceeding this temperature can cause undesirable effects in the electrical performance.

SYSTEM-LEVEL ANALYSIS USING FNM

In this section a brief description of the FNM technique is provided. More details of this methodology are described by Belady et al. [7] and Steinbrecher et al. [8]. FNM analysis consists of representing the flow system as a network composed of flow paths and components for the purpose of predicting system-wide distribution of flow rates and temperatures. Flow paths represent ducts or flow passages while components represent localized flow resistances. Each element of the system (flow path and component) is represented by overall flow and temperature characteristics that describe the variation of the pressure and temperature through that element with the corresponding flow rate. The following equation describes the variation of pressure drop with flow rate for each component:

$$\Delta p = k \frac{1}{2} \rho \left(\frac{Q}{A} \right)^2 \tag{5}$$

The loss coefficient for standard components such as ducts, area changes, screens, and bends can be obtained from handbooks such as Idelchik [10] and Blevins [11]. For nonstandard components supplier data, CFD analysis, or test data can be used to get the flow characteristics. Also, the Nusselt number (dimensionless heat transfer coefficient) for each component that participates in heat transfer can be described by the following empirical correlation:

$$Nu = a\, Re^m\, Pr^n \tag{6}$$

Flow and temperature characteristics for all elements constitute the momentum and energy equations respectively for the system. In addition, mass conservation is required at each junction in the flow network. The system of equations is solved using the SIMPLE algorithm of Patankar [12]. It involves update of the flow rates for each element using the existing pressures. This is followed by the construction and solution of the pressure correction equations at individual nodes. All nonlinearities in the momentum equations, such as dependence of pressure loss on the square of the flow are handled using iterations. The network analysis of the flow distribution in the units is carried out using a commercial program MacroFlow [13], which incorporates the FNM methodology in a generalized manner. Figure 3 shows the network representation of the 10 KW/25 kW units. Each part of the network directly corresponds to the relevant portion of the physical system. The network model for the 10 kW or 25 kW units is constructed by describing the paths followed by the air as it travels from the side inlets to the exhaust at the bottom of the units. The layout of the flow network model for the 10 kW and 25 kW units are identical, the differences between two models are only in the geometrical quantities and fan characteristics. As is described above, the units have four identical airflow paths from inlets at four sides of the unit through the resistor sections. Instead of modeling all four passages, MacroFlow allows us to model only one airflow passage and then apply a multiplier of four. This capability of the software not only reduces the modeling time substantially but also reduces the size of the network. These elements are identified in Figure 3 by a multiplier of four in the parenthesis. Note that the multiplier can be used only if the branches are geometrically identical and receiving identical flow rate. The flow enters the system through four openings at the side walls (AIR-INLET). The losses through these opening are represented using an inlet component that is exposed to the ambient pressure. The flow then moves through four air-moving devices (AMD) before entering the outer air-guides (OAG). The characteristics of the AMDs are specified from the data provided by the manufacturer. Flow experiences an area expansion between the AMD exhausts and OAG, producing a pressure loss in the flow. The main cause of the pressure loss is the formation of large re-circulating eddies in the corner regions as the flow expands from a smaller to a larger cross-section. These pressure losses are also available through empirical correlations from handbooks. The effect of the area expansion on the flow system is modeled by using the area expansion loss. The OAGs are modeled as ducts with noncircular cross sections and definite length. After the outer air guides, the flow turns 90 degrees and enters the inner chamber through perforated screens (RF_SCREEN) and turns another 90 degrees to enter the start of the resistor section (RESISTOR_LAUNCH). The screen is modeled using a screen component with a fractional clear area of almost 50%. Similar to the area expansion component, the screen component has access to the empirical correlations for the pressure drop across a screen. Therefore, by providing the fractional clear area of the screen and geometrical values of the holes in the screen the pressure drop across screen is calculated. The four identical flow branches merge at the resistor section (or resistor plenum) to a single flow branch, therefore, the rest of the flow network model does not have the multiplier of 4. The flow will then expand to the RF absorption structure (RF_INNER_HOUSING) where the resistors are located. The effective available cross sectional area and the wetted perimeter are calculated and used to model the RF inner housing as a duct with noncircular cross section. The flow then expands to the exhaust section (DUCT01), turns 90 degrees and leaves the system through a screen exposed the ambient pressure (EXHAUST).

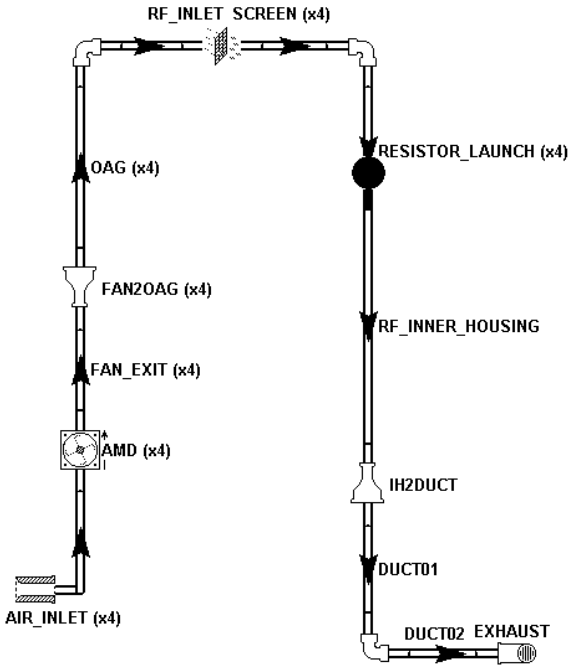

Figure 3. Network Representation of Physical System

Analysis of the flow network of these units provides information about the flow distribution and pressure losses throughout the system. Note that network analysis automatically accounts for the interaction between the system and impellers characteristics, thus, the impellers operating points are predicted from the analysis. Finally, due to the modular nature of the network representation, effect of changes to the system such as changing impellers or incorporation of a more open screen at the exit are readily carried out for efficient optimization of the thermal performance of the system.

DETAILED ANALYSIS USING CFD

The CFD technique provides a more detailed prediction of the velocity distribution, pressure distribution, and fluid and surface temperatures. The prototype system-level model of the scaled up load was modeled in I-DEAS Electronic System Cooling (ESC), a commercially available software package for electronics system cooling. [14]. ESC allows for rapid creation of the element mesh and boundary conditions directly from solid CAD data. I-DEAS ESC is an element based control volume CFD code that solves the 3D Navier-Stokes equations for flow and energy in the heat transfer processes. The physical and mathematical specifications of ESC can be found in the literature [15,16]. The following thermal phenomenon were modeled:

- Convection from the RF absorption media and RF housing
- Radiation from the RF absorption media to the wall of the inner chamber
- Conduction from the resistor ends to their support structures
- Exterior convection and radiation

Convection is modeled by using a thermal boundary layer model derived from Reynolds analogy. The approach makes use of the local distribution of velocities, shear stresses and the turbulence quantities in the near-wall region to calculate the convective heat transfer coefficient. The thermal conduction, convection and radiation simulation uses the finite control volume (finite difference) method to obtain the solution to the thermal model. It utilizes the unstructured finite element mesh to discretize the model. This method, also known as the lumped parameter method, is based on conservation of energy applied both locally and globally within the domain. Coupling of the thermal and flow solvers is performed by passing energy between the two solvers at the fluid/solid interface. ESC also allows for the creation of thermal couplings between elements that are not geometrically connected; that is a path for heat to flow between elements that do not share common nodes. The couplings are established based on proximity, and are distributed to account for overlap. Such a method allows complex paths to be modeled without defining complex geometry. This technique was utilized to model radiation to the inner housing and conduction from the resistor clips.

Figure 4 shows the CFD model for the whole physical system. Only the thin-shell elements are shown for clarity whereas the actual model had a tetrahedral fluid mesh throughout the entire calculation domain. The physical system readily lent itself to half-symmetry, allowing for a reduced number of elements generated. A symmetry boundary condition applied at the cut plane bounds the fluid to be tangential and does not include boundary layer drag. The absorptive structure was modeled using thin shells with half of the total heat load uniformly applied. This surface mesh and the fluid immediately surrounding the absorptive media were kept small to accurately predict convection heat transfer and the mesh density decreased as the fluid moved away from the resistor array. In the outer air guides (OAG), small flow velocities are observed and decreasing velocity is found as the fluid progresses to the exit through the duct/diffuser. The AMDs were affixed as a pressure-CFM boundary conditions which the program iteratively solved to find the operating point by taking an initial

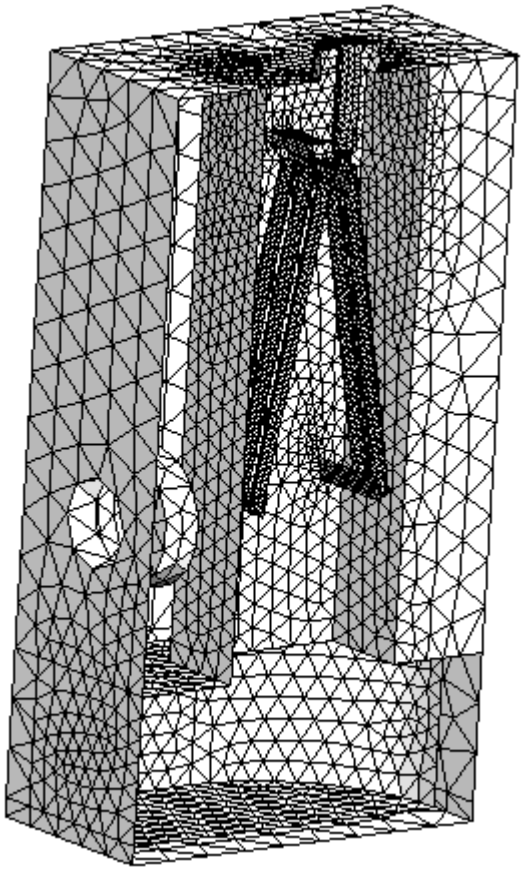

Figure 4. The CFD Model of the System

guess of .75 times the zero load CFM. Flow guides, baffles, walls, and resistor support structures were also modeled using the thin shell elements, which account for convection calculations on both sides when exposed to fluid. Conduction along the wall and along the resistors is accounted for by applying a thickness and thermal conductivity the shell elements. The exhaust vent and RF inlet screen are modeled as a pressure loss, the correlations taken from standard handbooks. The screen meshes do not participate in the conduction calculations. Tetrahedral elements formed the fluid mesh and 3-node thin-shell elements formed the dividing walls and resistors. A tetrahedral mesh was used since ESC contains powerful and rapid automatic tetrahedral mesh tools and the engineering-level analysis required made tetrahedral a logical choice. The final CFD model contained 97400 fluid elements, 21200 thermal elements and 28800 nodes.

PHYSICAL PROTOTYPE VALIDATION

To compare experimental results with predicted FNM and CFD results, prototype models of each unit were built and tested. Since each device under test (DUT) was a low-pass device, i.e. capable of absorbing power at very low frequencies, a 60 Hz line frequency power source was used to provide power to the load. The main goal of this study was to compare overall temperatures of the absorption media with those predicted by FNM and CFD. While the line frequency source does not simulate the attenuation characteristics discussed above, it did provide for a uniform power source which was duplicated in the FNM and CFD boundary conditions. Testing was performed at an ambient temperature of 25°C. Volumetric flow rate was determined by measuring the static pressure in each OAG chamber and finding the corresponding CFM value from supplied curves. The measurement error due to instrument error and curve interpolation was estimated to be 15 CFM. Bulk temperatures of the absorbing medium were verified using a non-contact measurement method since high-power, RF fields are a hostile environment for standard surface temperature measurement methods such as thermocouples and RTDs. The load was allowed to stabilize for 45 minutes while TCR drift was compensated by proportional feedback of input power, to within 200 watts. Measurement error by this method from instrument, sighting and power drift error was estimated at 35 ^{o}C.

RESULTS

To begin the investigation of scale-up from 10kW to 25kW, the FNM model was evaluated using data from the 10kW prototype. The FNM model of the baseline 10kW was built and solved at the standard condition of 25 °C and 1 atm ambient temperature and pressure. Since the RF inner housing area could not be increased to handle the increased CFM, it was initially important to verify CFM values as the system would be operating in a non-linear area of the system curve. The system curve for the baseline 10kw unit are shown in Figure 5 along with the 10kW AMD pressure-flow curves. The two 10 kW fan curves shown are for the same AMD but with different line frequency inputs. The AMDs used are designed to operate at both line frequency inputs but 50 Hz operation will result in a de-rating factor. The system curve was generated in the FNM model by applying various flow rates and obtaining the total pressure losses across the system. This was possible only due to the high speed of execution of the FNM model. The velocities through various parts of the system are shown in Figure 7. Also, Table 1 shows the volumetric flow rates through one of the AMDs. The total flow rate will be four times of the flow rate through one AMD.

As a first-pass scale-up iteration, the original AMDs in the 10KW FNM model were replaced with the larger AMDs to obtain a baseline operating point for the 25KW model. The 50 and 60 Hz pressure-flow curves for these AMDs (the potential AMDs for the 25kW unit) are also shown in Figure 5. The FNM model predicted 344 and 359 CFM for each of the 50 and 60 Hz AMDs respectively, which translates to the overall CFMs of 1375 and 1436 through the system. This initial pass would not meet the specification for the total volumetric flow rate of 1500 CFM through the system. Thus the components of high

pressure-drops were identified for design modification. Figure 6 shows the pressure losses through different parts of the system

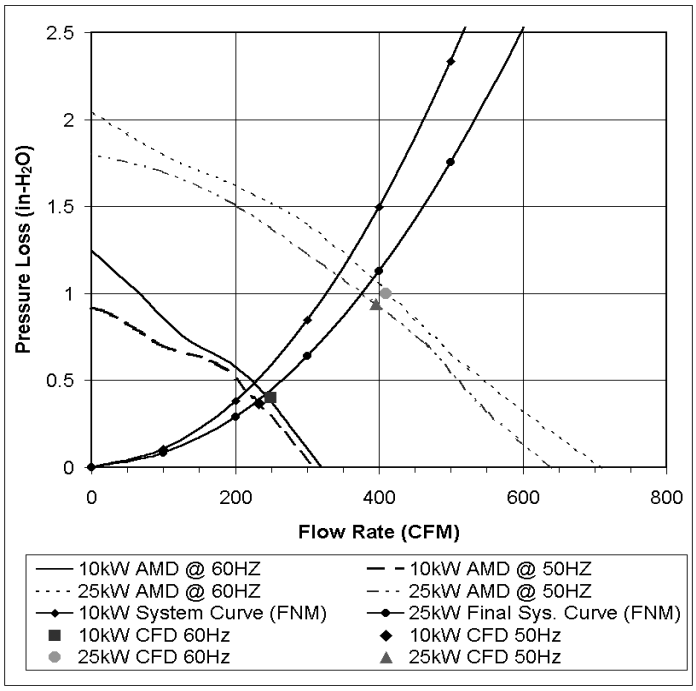

Figure 5. System curves and AMD characteristics

for the first-pass (using the AMDs for 25kW in the 10KW geometry). It can be seen that the maximum pressure drop occurs at the EXHAUST. The possible remedies to reduce the pressure drop at the exhaust are increasing the total exhaust area and increasing the Free Area (FA) of the screen at the exhaust. The baseline 10 kW EXHAUST had a FA ratio of 0.63. Manufacturing, structural, and EM shielding constrains placed limits on the size of the exit orifices and thus, the upper limit on FA was limited to 0.65. Therefore, the exhaust duct area (DUCT02) was increased by 28% and the orifice size was increased by 66% to maintain a FA ratio of 0.63. The OAGs were also scaled up 50% to handle the increased packaging of the larger AMDs, bringing the total package envelope to 27"L x 27"W x 60"H. This new scale-up design reduced the pressure drop of the EXHAUST by 29%. The pressure drops through different parts of the scale-up model are also shown in Figure 6. Notice that the pressure drop in some other parts of the system such as the RF_INLET_SCREEN was increased due to the increase of the total flow rate. The system curve for the new design (final 25kW) is also shown in Figure 5. The predicted volumetric flow rates are 383 and 397 CFM for each of the 50 and 60 Hz AMDs respectively, which translates to the overall CFM of 1532 and 1588 through the system. Therefore, the requirement of the minimum volumetric flow rate of 1500 CFM is satisfied. Table 1 summarizes the values of the volumetric flow rates for the 10KW Baseline and 25KW final scale-up designs. Also, the magnitudes of the average velocities through various parts of the system are shown in Figure 7. It can be seen that FNM predicts an average velocity of 11.3 m/s in the RESISTOR_LAUNCH section for the final 25kW design which meets its' specification for a minimum of 10 m/s velocity at the start of the resistive array.

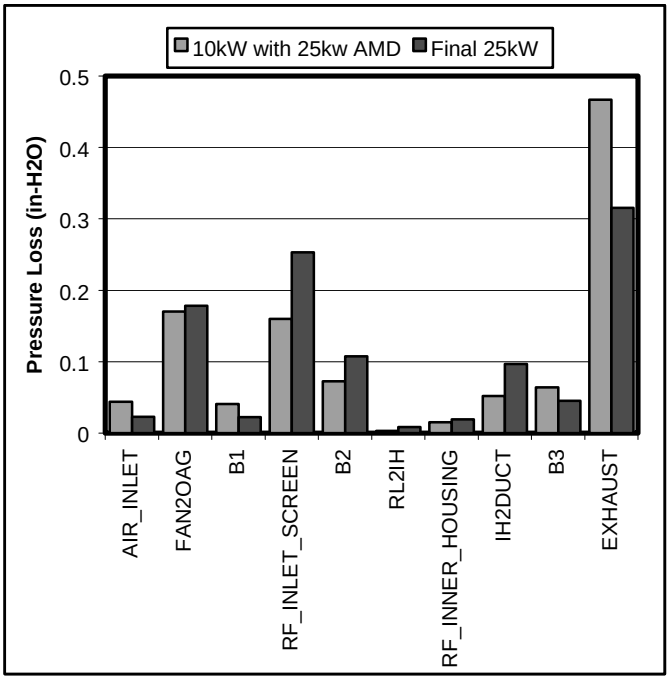

Figure 6. FNM Pressure drop; Initial & final 25kW scale-up

The results obtained from the FNM rapidly produced an optimized starting point to proceed with the detailed CFD investigation. Normally, the results presented above would have been obtained through laborious CFD calculations and numerous time-consuming re-builds of the model. The CFD model for the baseline 10KW and final 25KW designs were built and run. The comparison between the results obtained from FNM and CFD with the experimental measurements are shown in Table 1. It is shown that the difference between the overall flow rate obtained from FNM and CFD is always below 10%. CFD predicted volumetric flow rates that are higher than predicted by FNM and closer to the experimental results. In general, the flow rates predicted by CFD are within 5% of the measured flow rates while FNM predicts the flow rates within 11% of the measured values. Both prediction methods show that the 25 kW unit meets its' specification for a minimum of 10 m/s velocity at the start of the resistive array and total volumetric flow rate of 1500 CFM. The 50Hz FNM and CFD cases were simulated at 45 °C ambient while the experimental values were obtained at 25 °C and adjusted for the temperature difference. The effects due to temperature on the air properties are small compared to the measurement error.

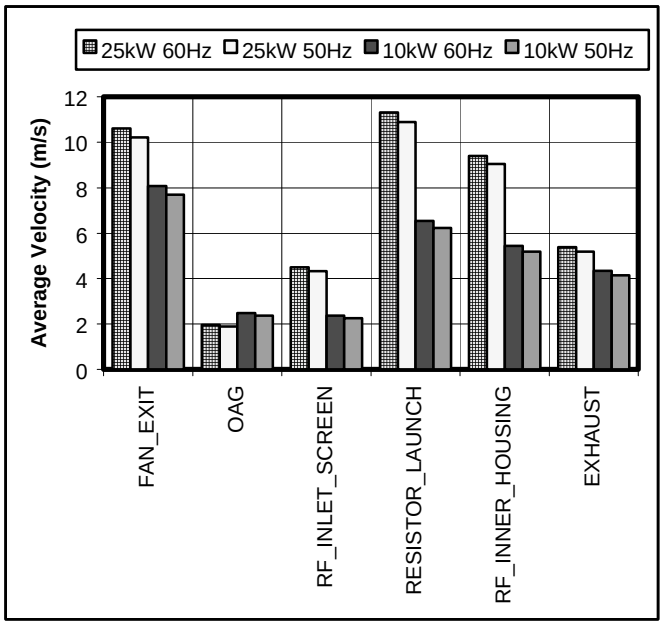

Figure 7: Velocities through Various Parts of the System Obtained from FNM Analysis

Table 1. Volumetric Flow Rates of One AMD for Various Cases

OAG VOLUMETRIC FLOW RATE (CFM)			
CASE	**FNM**	**CFD**	**EXP.**
10 kW Baseline (50 Hz AMD)	217	233	244
10 kW Baseline (60 Hz AMD)	227	249	250
25 kW Final Scale-up (50 Hz AMD)	383	395	399
25 kW Final Scale-up (60 Hz AMD	397	410	414

To calculate the resistor's surface temperature the energy equation was solved in both FNM and CFD models. A uniform heat load was considered over the resistor array. The CFD analysis provided more detailed information about the heat flow and surface temperature in various parts of the resistor array. CFD analysis showed that the convection heat transfer from the resistors surfaces is the dominant mode of heat transfer. The heat conduction from the resistor array bases and radiation to the surroundings contribute less than one percent of the total heat transfer. This is explained since the resistors are of a low conductivity ceramic and have a low shape factor for radiation coupling to the inner housing. This provides good support for FNM predictions of surface temperatures since in this FNM analysis the conduction and radiation effects were ignored.

Table 2 shows the average resistor temperatures as predicted by FNM and CFD compared with experiment. It can be seen that the temperature values predicted by FNM and CFD methods agrees well with the measured values, the difference being of the order of 10%. The 50Hz, 45 °C data was measured at 25 °C and adjusted for the temperature difference. It is important to note that in CFD analysis the heat transfer coefficient is calculated locally based on the fluid temperature gradient close to the surface while the FNM technique uses the available empirical correlations to calculate the heat transfer coefficient.

Table 2. Average Resistor Array Temperatures

AVERAGE RESISTOR SURFACE TEMP. (°C)			
CASE	**FNM**	**CFD**	**EXP.**
10 kW Baseline (50 Hz AMD, 45 °C Ambient Temperature)	310	302	271
10 kW Baseline (60 Hz AMD, 25 °C Ambient Temperature)	248	238	245
25 kW Scale-up (50 Hz AMD, 45 °C Ambient Temperature)	425	413	390
25 kW Scale-up (60 Hz AMD, 25 °C Ambient Temperature)	388	376	351

Table 3 shows the actual times for the FNM-CFD-Test method compared to the CFD-Test method as outlined in the introduction. The 10kW load was developed using the CFD-Test methodology and the 25kW load was developed using the FNM-CFD-Test methodology. The times presented in Table 3 consider the RF, thermal and CAD aspects of the designs. RF optimization and thermal validation involved testing with physical mock-ups. The CAE and physical optimization for the RF design were leveraged in the 25 kW unit which provided a 25 week total reduction in the development time. Considering only the FNM, CFD, and physical validation parts, a 4 week or 57% reduction in thermal design time was realized using the FNM-CFD-test methodology.

Table 3. Development Times (weeks)

Design Stages	**10 kW Baseline**	**25 kW Scale-up**
CAE RF Design	14	1
Thermal FNM	0	1
CFD	6	1
CAD & BOM	4	3
RF Optimization	6	0
Thermal Validation	1	1
Total Time	**32**	**7**

CONCLUSION

It is apparent from the above discussion that in the design of any high-power RF absorption load, there exists competing

trade-offs between the RF structure and the cooling system. The ease of construction of the FNM model and the speed of execution (seconds instead of hours for CFD) gave considerable insight into the scale-up issues that needed to be addressed by streamlining investigation of basic system parameters. This provided a reduction in time spent for both CFD modeling and prototype iterations and allowed the CFD efforts to focus on fine-tuning the design without delaying product roll-out. In general, it was shown that the agreement between results obtained from FNM and CFD analysis is very good. From this study we can expect volumetric flow rates predicted from FNM to be within 11% of measured values and CFD results within 5%. Surface temperatures are expected to be with 14% of experimental with FNM predictions and 11% from CFD methods. Leveraging the existing RF section allowed all electrical specifications to be met and predicted flow rate, internal velocities and absorption surface temperatures were realized in the high-power unit with the aid of the FNM-CFD-Test method. A final benchmark of 57% reduction in thermal development time was ultimately realized in this study.

ACKNOWLEDGMENTS

The authors would like to thank Jefferson D. Lexa and Tim Holt from Bird Electronic Corp., Suhas V. Patankar and Kanchan M. Kelkar from Innovative Research, Inc. for their input and manuscript review.

REFERENCES

[1] J. Witaker *et al.*, "Standard Handbook of Video and Television Engineering", McGraw-Hill, New York, 2000
[2] C. J. Kaiser, "The Resistor Handbook, 2nd Ed." CJ Publishing, KS, 1194
[3] J. Agnew, "Thick Film Technology", Hayden Co., NJ, 1973
[4] K. K. Schuegraf, "Handbook of Thin-Film Deposition Processes and Techniques", Noyes Publications, NJ, 1988.
[5] J. Dimitrios, "Exact Cutoff Frequencies of Precision Coax," *Microwaves*, June 1965, pp. 28-31
[6] C. H. Spaderna, "A New Formula for Attenuation in Coaxial Cables," *IEEE Transactions on Microwave Theory and Techniques*, Vol. MTT-12, No5, May 1964, pp. 363-364
[7] Belady C., Kelkar K.M., and Patankar S.V., 1999, "Improving Productivity in Electronic Packaging with Flow Network Modeling (FNM)," *Electronics Cooling*, Vol. 5, No. 1, pp. 36-40.
[8] Steinbrecher R., Radmehr A., Kelkar K.M., and Patankar S.V., "Use of Flow Network Modeling (FNM) for the Design of Air-Cooled Servers," Advances in Electronics Packaging, *Proceeding of the Pacific Rim/ASME Intersociety Electronics and Photonic Packaging Conference*, Vol. II, pp. 1999-2008, 1999.
[9] Minichiello, A., "Flow Network Modeling: A Case Study in Expedient System Prototyping," Proceedings of ITherm 2000, Las Vegas, May 2000, Vol. I, pp. 70-77.
[10] Idelchik I.E., 1994, "Handbook of Hydraulic Resistance", *CRC Press*, Florida.
[11] Blevins R. D., 1992, "Fluid Dynamics Handbook", *Krieger Publishing Company*.
[12] Patankar S. V., 1980, "Numerical Heat Transfer and Fluid Flow", *Hemisphere*, New York, 1980.
[13] MacroFlow Users Manual, 2000, *Innovative Research Inc*., Plymouth, MN 55447, USA.
[14] Maya Heat Transfer Technologies, "I-DEAS Electronic System Cooling - Users Guide", June 1996.
[15] Agonafer, D. and Free A., "Conjugate Model of a Pin-Fin Heat Sink Using A Hybrid Conductance and CFD Model Within an Integrated MCAE Tool", Eurotherm Seminar No. 45, September 1995
[16] J. A. Free, R. Russell, "Recent Advances in Thermal/Flow Simulation: Integrating Thermal Analysis into the Mechanical Design Process" Eleventh IEEE Semi-Therm Conference San Jose, CA, February 1995.